Cloud processing dominates the vertical profiles of aerosols in marine air masses over the Great Barrier Reef

Braga, Ramon C.; Rosenfeld, Daniel; Hernandez, Diana; Medcraft, Chris; Efraim, Avichay; Moser, Manuel; Lucke, Johannes; Doss, Adrian; Harrison, Daniel

DOI
10.1016/j.atmosres.2025.107928

Publication date
2025

Document Version
Final published version

Published in
Atmospheric Research

Citation (APA)
Braga, R. C., Rosenfeld, D., Hernandez, D., Medcraft, C., Efraim, A., Moser, M., Lucke, J., Doss, A., & Harrison, D. (2025). Cloud processing dominates the vertical profiles of aerosols in marine air masses over the Great Barrier Reef. *Atmospheric Research*, *315*, Article 107928. https://doi.org/10.1016/j.atmosres.2025.107928

Atmospheric Research 315 (2025) 107928

Contents lists available at ScienceDirect

Atmospheric Research

journal homepage: www.elsevier.com/locate/atmosres

Cloud processing dominates the vertical profiles of aerosols in marine air masses over the Great Barrier Reef

Ramon C. Braga [a,*], Daniel Rosenfeld [b], Diana Hernandez [a], Chris Medcraft [a], Avichay Efraim [b], Manuel Moser [c,d], Johannes Lucke [c,e], Adrian Doss [a], Daniel Harrison [a]

[a] Reefs and Oceans Research Cluster, National Marine Science, Southern Cross University, 2450 Coffs Harbour, Australia
[b] Institute of Earth Sciences, The Hebrew University of Jerusalem, Jerusalem, Israel
[c] Institute of Atmospheric Physics, German Aerospace Center (DLR), 82234 Oberpfaffenhofen, Germany
[d] Institute of Atmospheric Physics, Johannes Gutenberg-Universität, Mainz, Germany
[e] Faculty of Aerospace Engineering, Delft University of Technology, Delft, the Netherlands

ARTICLE INFO

Keywords:
Aerosol-cloud interactions

ABSTRACT

The cloud condensation nuclei (CCN) concentrations greatly determine the vertical microphysical evolution and rain initiation of warm convective clouds. We investigated the vertical profile of aerosol particles large enough (diameter > 60 nm) to act as CCN in marine air masses over the Great Barrier Reef. Such data were collected during an aircraft research campaign in February 2024. The results show a strong relationship between the microphysical processes measured in the cloud and the aerosol properties measured at the same altitude. The number concentration of aerosol particles decreases significantly above cloud bases due to CCN activation into cloud droplets. For heights above the in-cloud rain initiation level, the aerosol concentrations decrease further due to the scavenging of particles by drizzle and raindrops. The Hoppel minimum in particle size distributions is observed up to the altitude at which the coagulation process intensifies. Furthermore, a tail of larger aerosol particles was measured above the altitudes of rain initiation. These results suggest that the vertical profile of aerosols measured in marine air masses is dominated by cloud processing.

Plain text summary: Understanding the role of aerosol-cloud interactions is crucial information in accurately predicting the effects of climate change on the Great Barrier Reef (GBR). Characterizing the properties of aerosol particles found over the Reef is essential in determining their ability to act as cloud condensation nuclei (CCN). The evaporation of cloud droplets and raindrops represents an additional source that may influence the concentrations and sizes of aerosol. Here, we show that warm clouds dominate the vertical profiles of aerosol particles in the lower troposphere over the GBR. Our research shows that marine clouds work like a sink of aerosol particles found over the Reef. The cloud microphysical processes (activation of CCN into cloud droplets and the collision and coalescence processes) decrease the concentration of aerosol particles at the same altitude in the lower troposphere. Cloud processing develops the "Hoppel minima" or Hoppel minimum of the marine boundary layer aerosol size distributions as clouds evaporate. The Hoppel minimum is not observed in the particle size distributions above altitudes of intense coagulation processes. Above this level, the ultrafine particles dominate the aerosol concentrations.

1. Introduction

The interactions between aerosol particles and clouds represent a major remaining uncertainty in estimates of future climate (IPCC, 2021). The properties of aerosol particles control their ability to interact with solar and thermal radiation (direct effect) and act as cloud condensation nuclei - CCN (indirect effect). Except for polluted conditions with updraft limited activation, the number concentration of cloud droplets (Nd) at the bases of warm clouds mainly depends on the activation spectrum of the CCN as a function of the supersaturation over water (Sw) (Braga et al., 2021a; Braga et al., 2017; Reutter et al., 2009; Twomey, 1959). Above the cloud bases, the droplets grow by condensation, and in cases of small number concentrations (about 100 cm^{-3}), they coalesce quickly to form raindrops at low cloud depths $< \sim 400$ m (Braga et al.,

* Corresponding author.
E-mail address: ramon.braga@scu.edu.au (R.C. Braga).

https://doi.org/10.1016/j.atmosres.2025.107928
Received 19 August 2024; Received in revised form 2 January 2025; Accepted 14 January 2025
Available online 18 January 2025

2017; Freud and Rosenfeld, 2012; Gunn and Phillips, 1957; Konwar et al., 2012). The height of rain initiation within clouds is proportional to Nd at cloud bases, and thus, when droplet concentrations are larger, a slower increase in droplet sizes is observed during the condensational growth with height. The presence of Giant CCN (GCCN) (particles with sizes >1 μm) in air parcels would lead to the formation of relatively large cloud droplets near cloud bases that intensify the process of collision and coalescence, and thus, decreasing the height of rain initiation (Feingold et al., 1999; Gerber and Frick, 2012; Rosenfeld et al., 2002). In polluted cases (Nd $> \sim 500$ cm^{-3} at cloud bases), precipitation is formed at higher levels than clouds formed in clean air masses and can reach supercooled temperatures (Andreae et al., 2004; Braga et al., 2017; Rosenfeld et al., 2008).

Previous studies based on the analysis of aircraft and satellite measurements and cloud model simulations have described the effect of clouds on the aerosol properties measured around the clouds compared to cloud-free zones (Altaratz et al., 2013; Bar-Or et al., 2012; Eytan et al., 2020; Konwar et al., 2015; Koren et al., 2007). Koren et al. (2007) described the region around clouds as a *twilight zone*, "a belt of forming and evaporating cloud fragments and hydrated aerosols extending tens of kilometers from the clouds into the so-called cloud-free zone". The authors state that the gradual transition from cloud to dry atmosphere is proportional to the aerosol loading in the cloud, and it might affect about 30 % - 60 % of the free atmosphere by increasing the aerosol optical depths. Based on aircraft data collected during the Cloud Aerosol Interaction and Precipitation Enhancement Experiment (CAIPEEX) in India in 2011 (Kulkarni et al., 2012), Konwar et al. (2015) have explored the physical properties of near and far cloud aerosols and their impact on radiative forcing. The authors found that near the cloud edges, the aerosol effective diameter may increase by a factor of 2 compared to measurements far from clouds. The practical effect of the humidified aerosols near cloud edges is the increase of the reflected flux of solar radiation back to space and a decrease in the mean surface cooling compared to cloud-free regions. A recent study from Eytan et al. (2020) described, based on satellite measurements, the global radiative effect of the *twilight zone* from low-level clouds over the oceans. The study found that the average longwave radiative effect of the twilight zone is about 0.75 W m^{-2}, which is equivalent to the radiative forcing from increasing atmospheric CO_2 by 75 ppm, or 60 % of the CO_2 increase in the atmospheric column since the pre-industrial period. This effect extends up to ~11 km from detectable clouds, with over 90 % of the effect confined to a belt within ~4 km around the clouds.

In our previous study, (Braga et al., 2022), we focused our analysis on understanding the physical processes of aerosol-cloud interactions near convective ice-free clouds over the Amazon basin. Through airborne measurements conducted with the German HALO aircraft, we demonstrated that the CCN particles located at the lateral boundaries of non-precipitating convective clouds primarily derive from evaporated cloud droplets. The turbulent mixing in cloud bases causes the entrainment of CCN particles from lower levels, resulting in their activation into cloud droplets. Particles ingested from below cloud bases evaporate at the lateral boundaries above the cloud base, transforming into CCN particles again. The concentration of CCN is reduced when smaller droplets are removed through collision and coalescence processes. This also decreases the number of detrained droplets that evaporate outside of clouds. The formation of larger CCN particles around clouds directly results from the evaporation of larger droplets released from clouds above the height of coalescence initiation. Notably, non-precipitating convective clouds primarily produce CCN particles at their edges, which are the residues of the evaporated cloud droplets. Conversely, CCN concentrations in the atmosphere decrease considerably due to scavenging by rain resulting from drop coalescence in precipitating clouds. When a high concentration of CCN particles is significant from long-range transport above cloud base heights, the impact of convective clouds in the discharge of CCN particles at their lateral boundaries is overshadowed by the excess CCN particles.

In this study, we performed a similar analysis of the vertical distribution of aerosol particles for background conditions in which the marine air masses affect cloud formation and development. The measurements were performed at the Great Barrier Reef (GBR) in the region of Gouda Reef (16.43°S, 157.04°E), onboard a research aircraft during the Marine Cloud Brightening (MCB) campaign in 2024 (Hernandez-Jaramillo et al., 2024). We researched aerosol particles using an Ultra-High Sensitivity Aerosol Spectrometer (UHSAS) (Cai et al., 2008; Moore et al., 2021) to measure their vertical profiles. The UHSAS measurement range includes particle size diameters (d) that are crucial for the formation of warm clouds (60 nm $< d <$ 1000 nm) (Braga et al., 2022; Haarig et al., 2019; Mamouri and Ansmann, 2016; Rogers and Yau, 1989). As in the Amazonian study, the aerosol particles were measured at low relative humidities (< 40 %) to prevent the high variability of aerosol sizes due to the environmental humidity. A Cloud Combination Probe (CCP) was used to measure the cloud properties. The CCP combines multiple individual instruments, including a Cloud Droplet Probe (CCP-CDP) and a grayscale Cloud Imaging Probe (CIPgs) (Baumgardner et al., 2001). Combining the CDP and CIPgs allows cloud particles from 3 μm to 960 μm to be analyzed, which covers the measurements of cloud droplets and precipitating particles (drizzle drops and raindrops) (Braga et al., 2021b; Lucke et al., 2022; Moser et al., 2023).

Over GBR, marine aerosols have an important effect on mitigating the coral's physiological stress by reducing surface solar irradiance and sea surface temperature (Eckert et al., 2024; Jackson et al., 2020; McGowan et al., 2022). Aerosol particles with diameters smaller than 0.1 μm are predominantly formed through heteromolecular homogeneous nucleation. These particles are composed mainly of oxidation products of dimethyl sulfide (DMS) (Andreae and Raemdonck, 1983; Jackson et al., 2020; O'Dowd and de Leeuw, 2007). DMS is oxidized primarily by hydroxyl radicals (OH), nitrate radicals (NO_3), and halogen species such as bromine oxide (BrO) and chlorine radicals. These reactions produce intermediates like sulfur dioxide (SO_2), sulfuric acid (H_2SO_4), and methane sulfonic acid (MSA), which play critical roles in aerosol nucleation and growth (Chen et al., 2018; Wollesen De Jonge et al., 2021). The production of MSA and H_2SO_4 particularly enhances particle formation in the marine boundary layer. Furthermore, aerosols formed from DMS oxidation serve as CCN, influencing cloud albedo and, thus, the regional radiative balance. Fine and ultrafine aerosol particles may also result from the oxidation products of organic vapors (Volatile organic compounds - VOCs) and can produce CCN mostly in the Aitken mode size range (Andreae and Crutzen, 1997; Swan et al., 2016). Over the Reef, large marine aerosol particles (d > 0.1 μm) result mainly from cloud processing and sea spray (Eckert et al., 2024; Jackson et al., 2020; McGowan et al., 2022). Aerosol particles from sea spray, generally larger than 0.5 μm, are produced depending on surface wind speeds over oceans and may contain organic material (Andreae and Rosenfeld, 2008; Hoppel et al., 1990; Quinn et al., 2017; Wex et al., 2016). Another important characteristic of sea spray is the production of GCCN (Feingold et al., 1999; Rosenfeld et al., 2002). The presence of GCCN during cloud droplet formation at the cloud base can lead to a faster formation of raindrops due to both the rain embryo effect and the competition effect, which reduces cloud base maximum supersaturation and consequently reduces the number of droplets activated.

During the aircraft campaign over GBR, we measured a characteristic bimodal aerosol size distribution from marine air masses with relatively low concentrations below cloud-based altitudes (Gong et al., 2019; Hoppel et al., 1986, 1990; Quinn et al., 2017; Wex et al., 2016). Hoppel et al. (1990) described that the major factor in shaping the bimodal submicron aerosol size distribution is associated with the cycling of aerosol particles, which are frequently observed at the top of the marine boundary layer. Cloud-processed aerosols are formed from repeated formation and evaporation of cloud droplets, resulting in CCN particles at the boundary layer. In the cloud stage, cloud droplets may absorb trace gases, altering their composition and the size of the resulting CCN

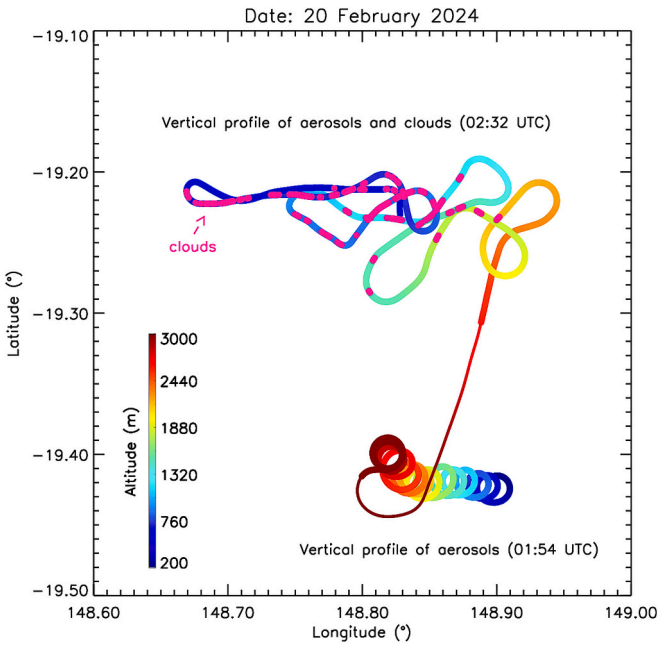

Fig. 1. Strategy of aerosol and cloud vertical profile measurements on 20 February 2024. The colors indicate the altitude of the aircraft. The thicker lines indicate the region of aerosol and cloud measurements. The region of background aerosol measurements is shown at the bottom of the map. The aerosol measurements near clouds were performed with a horizontal distance of at least 1 km of cloud elements. Cloud passes are indicated in pink. The prevailing wind directions at 500 m, 1500 m and 3000 m were *E*-SE, E-SE, and E, respectively. (For interpretation of the references to color in this figure legend, the reader is referred to the web version of this article.)

after evaporation. Furthermore, smaller interstitial particles are captured by cloud droplets, decreasing the concentrations of particles too small to act as CCN. These processes cause an increase in the mass of the cloud-processed CCN and create a minimum in the size distribution (i.e., Hoppel minimum), which separates CCN particles (Accumulation mode sizes; $\sim 100\ \text{nm} < d < 1\ \mu\text{m}$) from interstitial particles (Aitken mode sizes; $\sim 10\ \text{nm} < d < 100\ \text{nm}$).

The in situ measurements of boundary layer clouds coupled with the underlying marine boundary layer over GBR exhibited similar microphysical characteristics of convective clouds found in different regions of the globe (e.g., Amazon, Atlantic Ocean, Israel, and India) (Braga et al., 2017; Freud and Rosenfeld, 2012; D. Rosenfeld, 2018). During our flights, trade wind cumuli generally covered the sky, and the effective radius of the cloud droplets increased with height above the cloud base at a nearly adiabatic rate, reflecting the near-extreme inhomogeneous nature of the mixing. The rain initiation due to collision and coalescence processes started at low cloud depths (~500 m) for the cleaner cases. The coagulation processes are significant and form warm rain when the r_e exceeds ~12 μm (due to large aerosol particles below cloud bases, possibly GCCN from sea spray), and fully develop when r_e exceeds ~14 μm. When aerosol concentrations were relatively higher below cloud base heights, the rain initiation started at higher cloud depths due to a slower increase in droplet sizes during condensational growth with height.

The following sections present the data and methodology applied to investigate the role of clouds in the vertical profiles of aerosols measured at GBR. We describe the relationship between the characteristics of the aerosol particle size distributions (PSDs) and the cloud processes measured at the same altitude. The results show how the activation of aerosol particles into cloud droplets, the condensational growth of droplets, and the collision and coalescence processes affect the observed vertical profiles of aerosols in the lower troposphere.

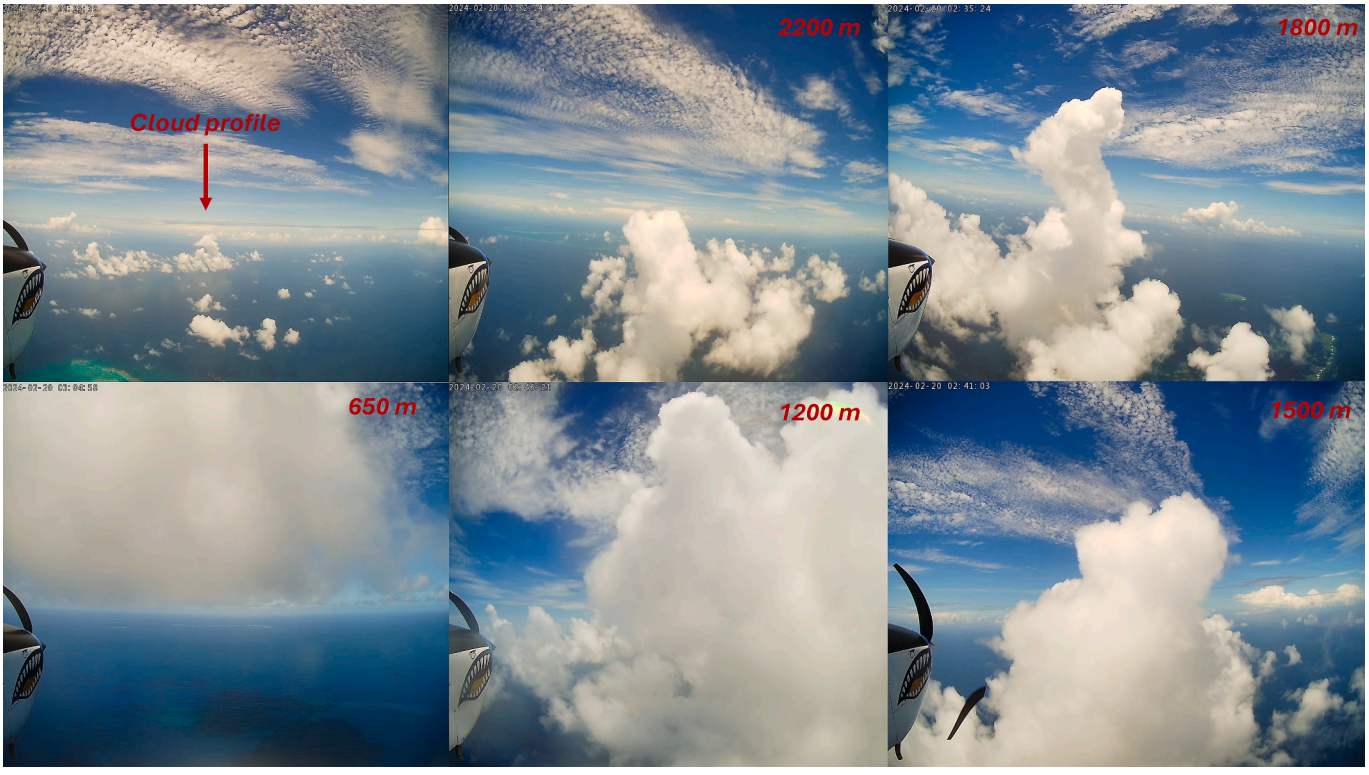

Fig. 2. Images from the camera below the aircraft's right wing during the cloud profiling on 20 February 2024. The altitude of cloud passes is shown in the upper-right corner.

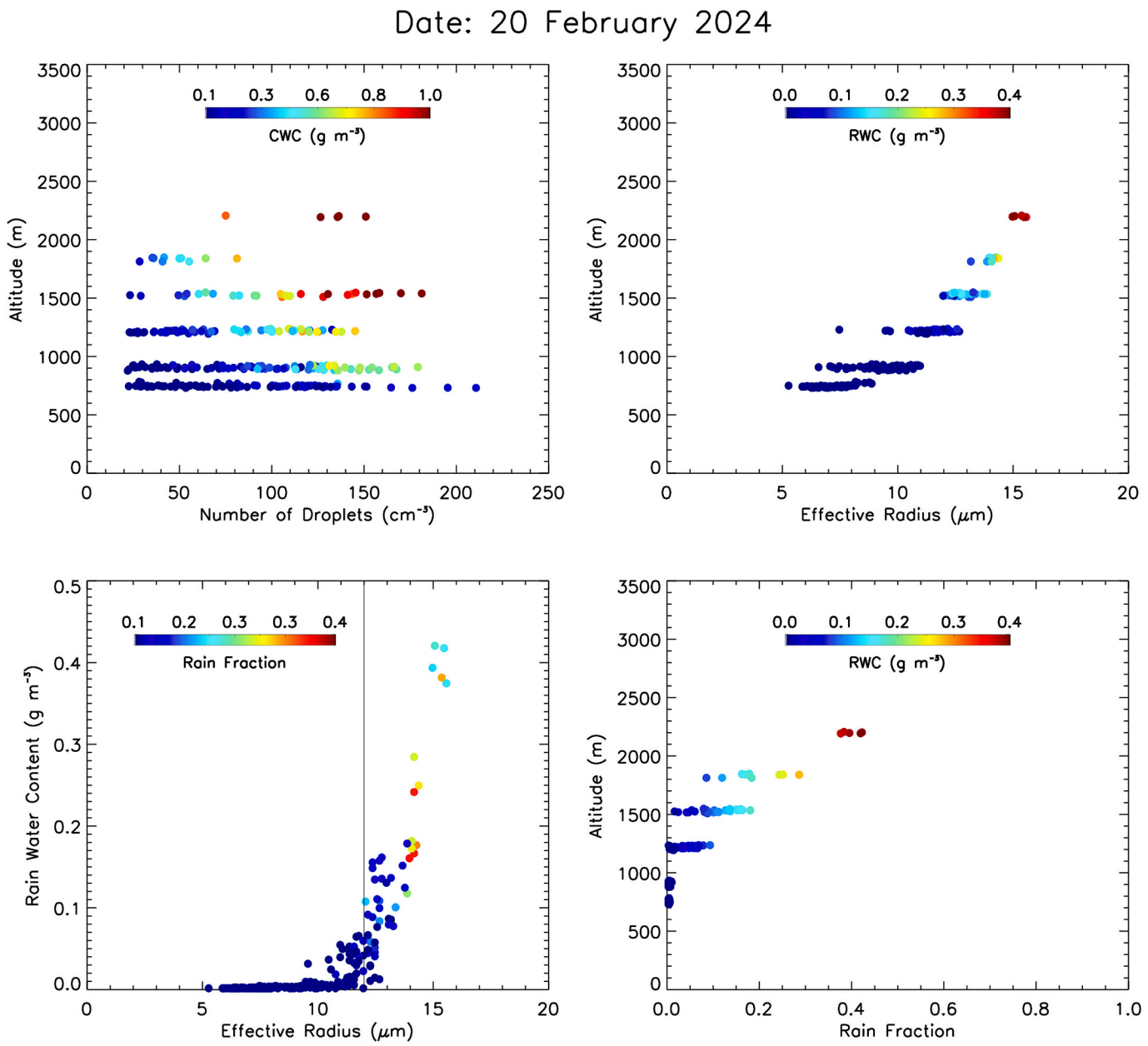

Fig. 3. Vertical profile of cloud droplet number concentration [upper-left], cloud droplet effective radius (r_e) [upper-right], r_e vs. Rain Water Content (RWC) [lower-left], and rain fraction as a function of altitude [lower-right] measured on 20 February 2024. Cloud Water content (CWC), RWC, and rain fraction [i.e., RWC / (CWC + RWC)] are color-coded in the panels.

2. Methods

The research aircraft used during the 2024 campaign for aerosol and cloud microphysics sampling was a Cessna 337, with the instrumentation setup detailed fully in Hernandez-Jaramillo et al. (2024). Briefly, the aircraft had a meteorological sensor system, AIMMS-30 (Aircraft Integrated Meteorological Measurement System), incorporating an ARIM-200 Air Data Probe mounted under the left wing. The AIMMS-30 provides temperature, relative humidity, and wind speed data with an estimated uncertainty of 0.3 °C, relative humidity at 2 %, and 0.5 m s^{-1}, respectively.

The UHSAS was mounted inside the aircraft cabin and supplied with air sampled by an isokinetic inlet located under the right wing. The measurements were collected for altitudes up to 10,000 ft. (~ 3200 m; ~9 °C). The vertical aerosol profiles were performed in the region around Gouda Reef. The profile consisted of a vertical ascending spiral flight maneuver to establish the background conditions of aerosol concentrations as a function of height. The ascending spiral was performed out of clouds as far as practical while measuring the background aerosols. For measurements around clouds, a horizontal distance of about 1 km was excluded from our analysis due to cloud contamination. Furthermore, only aerosol measurements in which the number concentration of droplets measured with CCP-CDP was smaller than 0.2 cm^{-3} were used in our analysis. A similar strategy was applied in our previous study in the Amazon region (Braga et al., 2022). The CCP was installed under the aircraft's left wing and was used to measure the cloud properties in the vicinities of aerosol measurements. The back trajectories from NOAA's Hybrid Single-Particle Lagrangian Integrated Trajectory model (HYSPLIT) (Stein et al., 2015) were used to characterize the long-range source of aerosol particles during the aerosol measurements. The following subsections describe the characteristics of aerosol and cloud measurements.

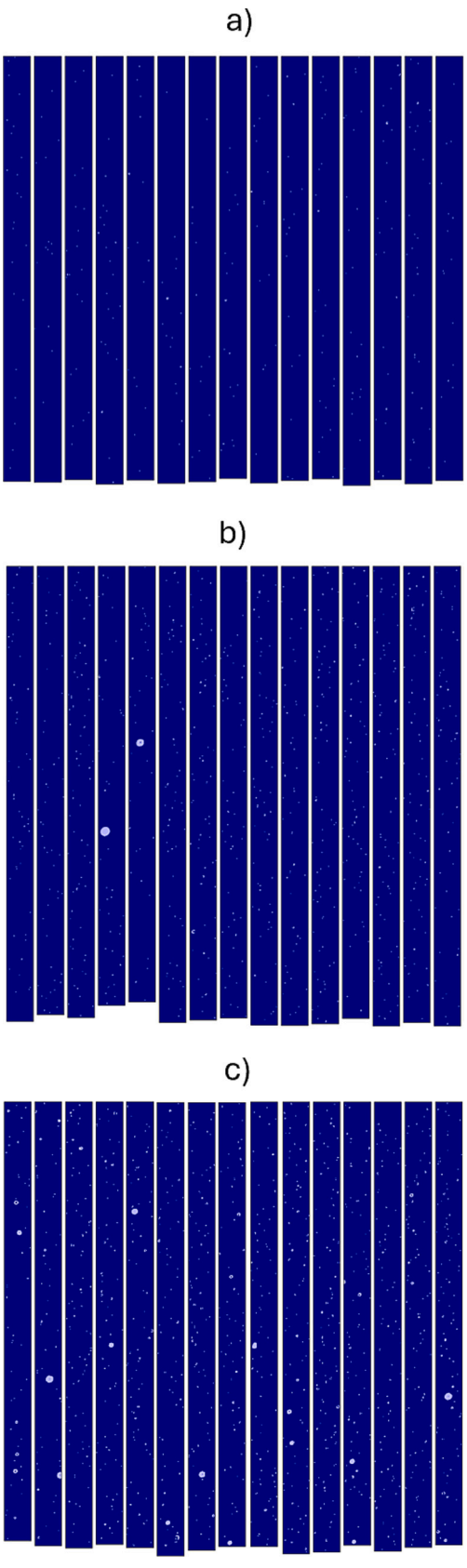

Fig. 4. CCP-CIP images at a) cloud base (~ 740 m a.s.l.) and b) ~ 1220 m when drizzle droplets start to be measured, and c) when coalescence is intense (~ 1800 m). The width of the CCP-CIP images is 0.96 mm.

2.1. Aerosol measurements

The UHSAS measured particles between 60 and 1000 nm in the diameter size range with 1 Hz frequency (Cai et al., 2008). The probe combines a high-power infrared laser ($\lambda = 1054$ nm) and a large solid angle range in a side-ways direction to detect light scattered by individual particles. The sampling inlet was mounted in an under-wing pod. The sampled air is entered into the instrument by a forward-facing diffusor inlet with a computer-controlled flow to create an isokinetic sampling of ambient air. Within the body of the isokinetic inlet, a pair of second inlets subsample the reduced velocity airflow at approximately matched velocity. The measured particle diameter is assumed to be the dry diameter since the air passed through two Nafion driers before being measured by aerosol probes. Relative humidity was monitored at the inlet of the instrumentation and maintained between ~ 20 % - 40 % during the measurements (this is typically below the efflorescence point for NaCl).

Before the aircraft campaign, the UHSAS was calibrated with monodisperse polystyrene latex spheres of known size at DMT (Droplet Measurement Technologies, Inc., Longmont, CO, USA). Typical uncertainties of UHSAS measurements are 15 % in diameter and concentration (Cai et al., 2008; Kupc et al., 2018; Moore et al., 2021). Only UHSAS measurements outside of clouds (Nd < 0.2 cm^{-3}) were used in our analysis. We performed smooth maneuvers during research flights to avoid contamination due to the aircraft's exhaust. In our flight tests, before the field campaigns, we observed that aerosol particles from the exhaust were measured in relevant concentrations for roll angles greater than 30° when rapid maneuvers were performed. In our analysis, we believe the contribution of exhaust particles is negligible. Furthermore, the undersizing of particles by UHSAS measurements due to absorbing (e.g., black carbon) is unlikely since we are analyzing the relative changes in concentrations and shape of the aerosol PSD. The average PSDs were calculated for at least 20 s of measurements (about 1 km in horizontal distance). The standard error of the mean PSD measurements in this manuscript varied from about 10 % to 30 %. These values depend on the measurement size range.

The total concentrations of UHSAS were compared with two Mixing Condensation Particle Counter-MCPC (Models 1720 and 9403) (Lopez-Yglesias et al., 2014; Wang et al., 2002). As expected, the UHSAS size-integrated number concentrations consistently measured fewer particles than those obtained by the MCPCs. This occurs because the UHSAS only encompasses a fraction of the complete spectrum of particle sizes (d $> \sim 10$ nm) that the MCPCs can measure.

2.2. Cloud droplet measurements

The cloud droplet number concentration and particle size distribution were measured at 1 Hz by a Cloud Combination Probe (CCP), which was mounted below the left wing of the research aircraft. The CCP combines two individual instruments, a Cloud Droplet Probe (CCP-CDP) and a grayscale Cloud Imaging Probe (CIPgs). The CDP counts the number of cloud particles and determines their individual size (detection range 3–50 μm) from the intensity of the forward-scattered laser light. The CIPgs detect larger particles from 15 μm to 960 μm, and the particle sizes are reconstructed from 2D shadow images using the shadowgraph technique (Baumgardner et al., 2001). The data processing was done with the software SODA [Software for OAP Data Analyses; (Bansemer, 2023)] using standard methods for liquid cloud processing [similar to what is applied in (Moser et al., 2023)]. Combining the CDP and CIPgs allows cloud particles from 3 μm to 960 μm to be analyzed [e.g., (Braga et al., 2017, 2021b; Lucke et al., 2022; Moser et al., 2023). This study also used the size and shape information from the CCP to identify rain droplets within the clouds.

Both probes performed measurements at a temporal resolution of 1 s, thus covering between 40 m and 50 m of horizontal distance. Cloud passes were defined for conditions under which the number of droplet

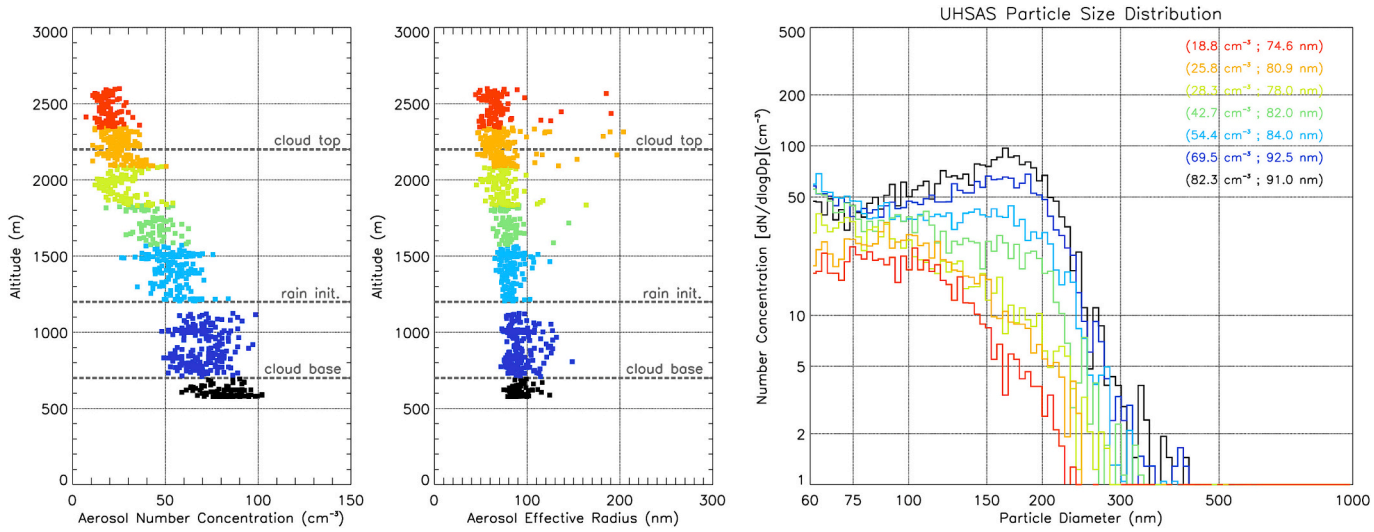

Fig. 5. Vertical profile of aerosol number concentration [left], effective radius [center], and average particle size distribution [right] as a function of altitude (indicated by colors) measured by UHSAS around clouds on 20 February 2024. The dashed lines indicate the altitude of cloud bases, rain initiation, and cloud tops (shown in Fig. 2). The mean number concentration of particles and aerosol effective heights are shown on the upper-right side of the right panel.

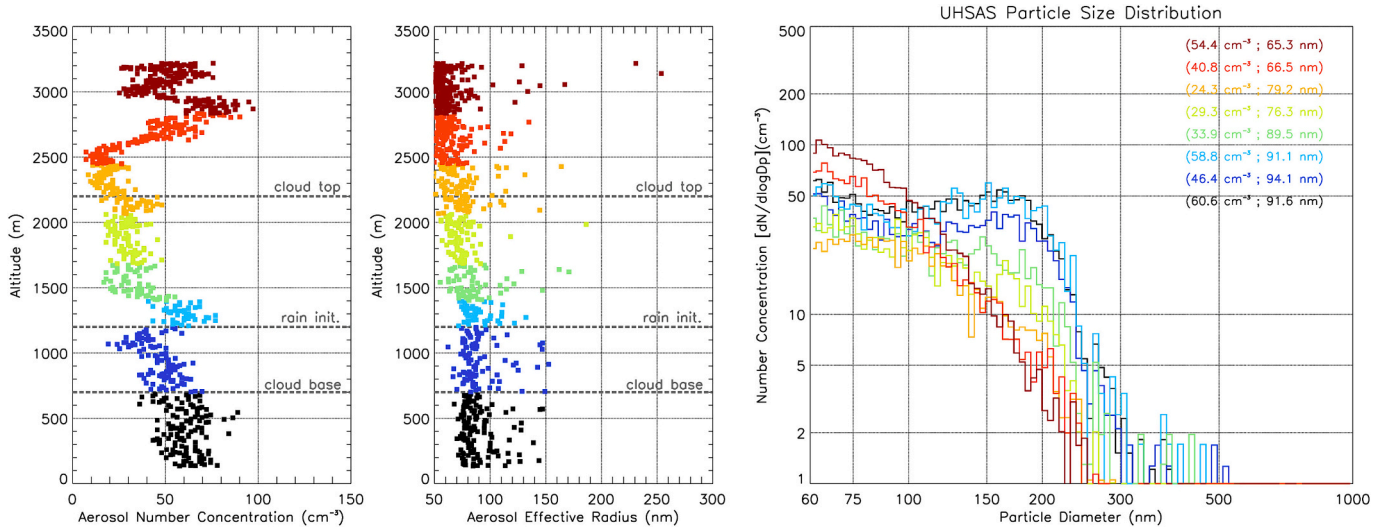

Fig. 6. Similar to Fig. 5 for background conditions for the same flight on 20 February 2024.

concentration (i.e., particles with a diameter larger than 3 μm) exceeded 20 cm^{-3} (Braga et al., 2021a; Campos Braga et al., 2017; Kirschler et al., 2023). This criterion was applied to avoid cloud passes well mixed with sub-saturated environment air (RH < 100 %) and counts of haze particles, typically found at cloud edges. The cloud passes were usually performed in different legs with a vertical distance of about 500 ft. (150 m). A variability of ~ 50 ft. could occur for the same cloud leg due to the turbulence within clouds.

Before the aircraft campaign, standard methods using monodisperse glass beads for calibrating the CDP were applied by DMT (Lance et al., 2010). Additionally, calibrations with glass beads of five different sizes (5.3 μm, 8.1 μm, 32.5 μm, 42.3 μm, 49.3 μm) were performed between the research flights to monitor the stability of the size bin classification. The uncertainties in particle sizing of CCP-CDP measurements have shown uncertainties smaller than 10 % during the campaign. Similar low uncertainty was found for the liquid water content estimated by the mass of the drops integrated over the diameter range of 3–50 μm and measured by a Kingprobe-type device (King et al., 1978) mounted on the CCP. During the campaign, measurements with the spinning disk calibration tool from DMT were regularly taken to check the CIP's functionality and consistent resolution.

2.3. Calculations of aerosol and cloud properties from airborne probes

2.3.1. Aerosol properties calculated from UHSAS particle size distribution

- Number concentration of aerosols (Na – [cm^{-3}]):

$$Na = \int_{30nm}^{500\ nm} N(r)dr \tag{1}$$

- Aerosol effective radius (Ar_e – [nm]):

$$Ar_e = \frac{\int_{30\ nm}^{500nm} r^3 N(r)dr}{\int_{30\ nm}^{500nm} r^2 N(r)dr} \tag{2}$$

where N is the particle number concentration, and r is the particle radius.

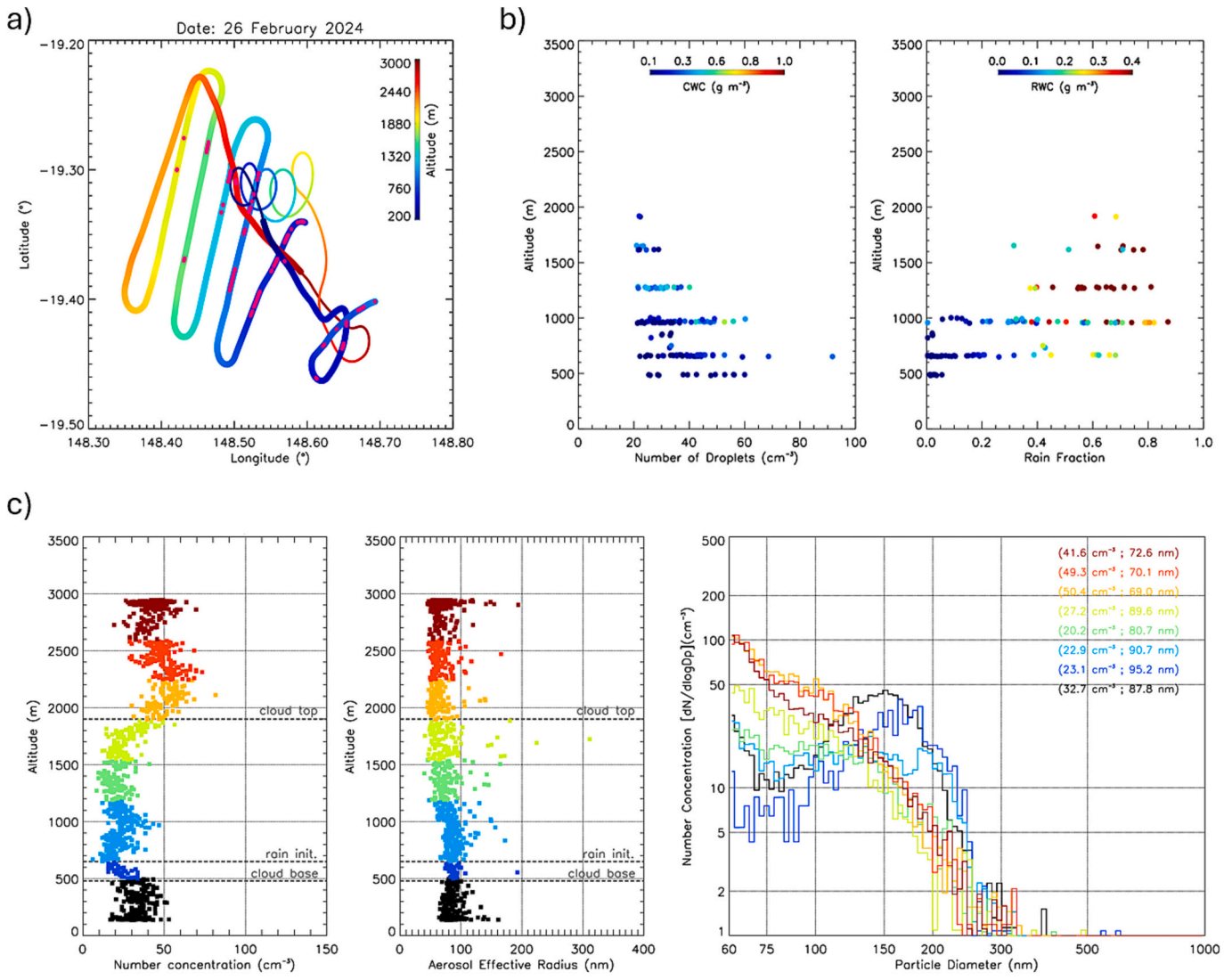

Fig. 7. a), b), and c) Similar to Figs. 1, 2, and 3 (respectively) for measurements on 26 February 2024. The prevailing wind directions at 500 m, 1500 m, and 3000 m were S-SE, SE, and NE, respectively.

2.3.2. Cloud microphysical properties calculated from CCP droplet size distribution

- Number concentration of cloud droplets (Nd – [cm^{-3}]):

$$Nd = \int_{1.5\mu m}^{25\mu m} N(r)dr \tag{3}$$

- Cloud droplet effective radius (r_e – [μm]):

$$r_e = \frac{\int_{1.5\mu m}^{25\mu m} r^3 N(r)dr}{\int_{1.5\mu m}^{25\mu m} r^2 N(r)dr} \tag{4}$$

- Cloud Water Content (CWC):

$$CWC = \frac{4}{3}\pi \int_{1.5\mu m}^{25\mu m} r^3 N(r)dr \tag{5}$$

- Rain Water Content (RWC):

$$RWC = \frac{4}{3}\pi \int_{25\mu m}^{480\mu m} r^3 N(r)dr \tag{6}$$

where N is the droplet number concentration, ρ is the density of water, and r is the droplet radius.

3. Results

During the research flights, we observed cumulus and stratocumulus clouds dominating the sky above GBR. The cloud profiling flights measured the cloud microphysical properties from cloud bases to the top to evaluate the effect of the cloud processes of condensational growth and collision and coalescence in the vertical profiles of aerosol particles. The vertical aerosol profile was performed for altitudes from below cloud bases up to above the top of clouds. Here, we show the results of measurements performed during four days of the aircraft campaign. On these days, clouds in different stages of development were measured, and the vertical profiles of aerosols are discussed addressing the effect of cloud processing on the measured aerosol profiles.

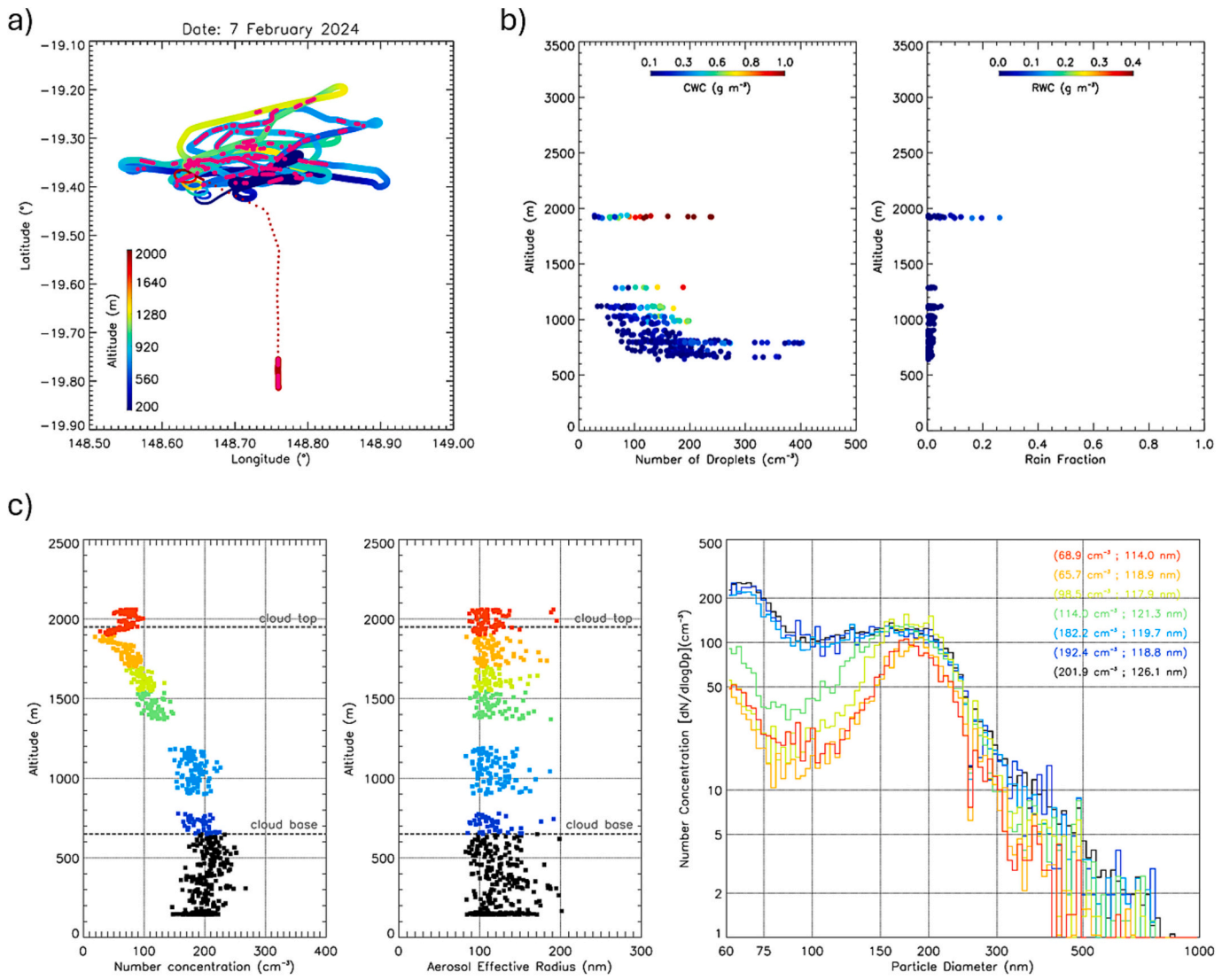

Fig. 8. a–c. Similar to Fig. 7a-c for measurements on 7 February 2024. The prevailing wind directions at 500 m, 1500 m, and 3000 m were S-SW, SE, and SE, respectively.

3.1. 20 February 2024

Fig. 1 shows the region of aerosol and clouds vertical profile measurements on 20 February 2024. On this day, the cloud properties of growing convective cumuli were measured from the cloud top to cloud base altitudes (cloud images are shown in Fig. 2). The vertical profiles of aerosols were performed around clouds and in the south of the cloud's region (background conditions), which developed on marine air masses from easterly winds (see Fig. S1).

Fig. 3 shows the microphysical properties of the convective clouds. The cloud base was measured at ~ 740 m a.s.l. at a temperature of ~21 °C. Given the clean conditions over the ocean, the high relative humidity and the low concentration of CCN lead to the formation of few and large droplets close to the cloud base (number concentration – Nd < ~200 cm^{-3}; and r_e ~5–8 μm). The rain initiation due to collision and coalescence processes starts at low cloud depths (~ 500 m). In this flight, drizzle droplets were imaged by CCP-CIP above 1200 m (see Fig. 4). The rate of coalescence process within the cloud can be ascribed by the conversion of cloud water (CWC) into rainwater (RWC) or the rain fraction [i.e., RF = RWC/(CWC + RWC)] (Braga et al., 2021b), and in this case, it starts growing linearly with height above 1200 m.

Fig. 5 shows the vertical profile of aerosol number concentration (Na), aerosol effective radius (Ar_e), and the average particle size distributions (PSDs) measured with UHSAS around the convective cumuli. The figure describes the vertical evolution of aerosol particles as a function of the cloud properties measured. Below cloud bases, the PSDs show a typical bi-modal shape with a Hoppel minimum at a diameter of about 75 nm. Na and Ar_e generally decreased with altitude due to droplet activation and collision and coalescence processes. Slight increases in the Ar_e are observed between cloud bases and the altitude of rain initiation (where the condensational growth of cloud droplets prevails). When the collision and coalescence processes are intensified, large values of Ar_e are observed due to the detrainment of large raindrops (especially near cloud-top altitudes).

The vertical profile of average PSDs shows that the concentration of accumulation mode particles decreases significantly above the level of rain initiation. Furthermore, the Hoppel minimum is observed up to the altitude at which the collision and coalescence processes are intensified (~ 1800 m). The PSDs from the boundary layer up to the cloud top level typically show a tail with low concentrations for diameters larger than 300 nm. This suggests these particles result from evaporated droplets after the cloud processing (condensation and coagulation). The Nd measured by the cloud probe exceeds by a factor of ~2–3 the Na measured in different altitudes, indicating that Aitken mode particles

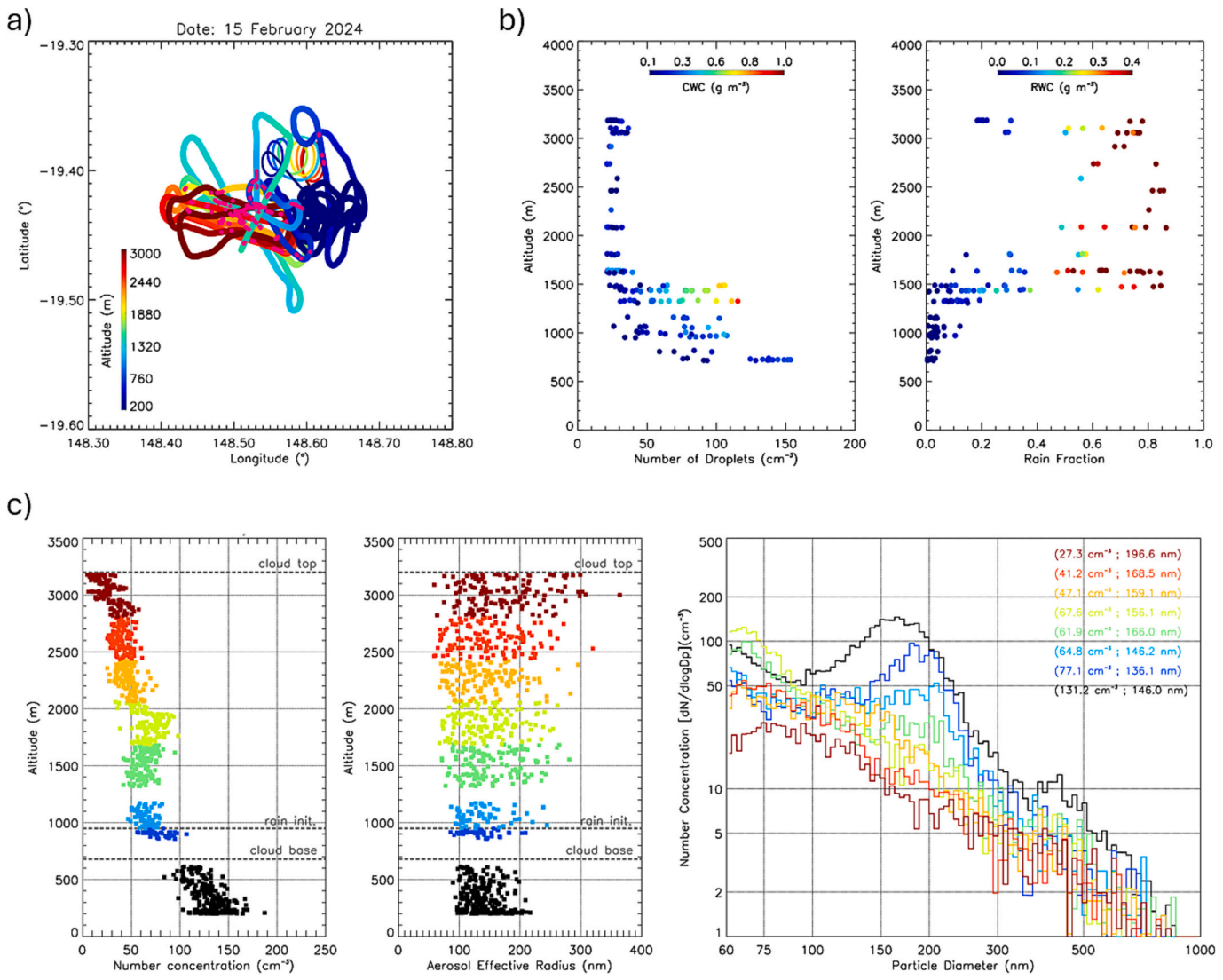

Fig. 9. a–c. Similar to Fig. 7a-c for measurements on 15 February 2024. The prevailing wind directions at 500 m, 1500 m, and 3000 m were *E*-SE, E-NE, and N-NE, respectively.

with $d < 60$ nm were activated into cloud droplets (see Fig. S2 for the total concentration of particles measured with UHSAS and CPC during this flight).

Fig. 6 shows that similar characteristics of aerosol properties were measured during the vertical profiling for background conditions without clouds (to the south of the clouds sampled region). The measurements above cloud top altitudes show an increase in the aerosol concentrations above cloud top. The aerosol properties suggest that these particles also result from cloud processes of precipitating clouds since the Ar_e shows similar characteristics of the measurements around clouds.

3.2. 26 February 2024

Fig. 7a shows the region of aerosol and cloud vertical profile measurements on 26 February 2024. The cloud properties of convective clouds were measured from the cloud base to cloud top altitudes (see Fig. S3). The vertical profiles of aerosols were performed around clouds that developed on marine air masses (see Fig. S4).

On this day, clean clouds were measured (Nd $< \sim 100$ cm^{-3}), and raindrops started to develop at low cloud depths (see Fig. 7b). Fig. 7c shows the vertical profile of Na, Ar_e, and the average PSDs measured with UHSAS around the convective clouds. Below cloud bases, the PSDs show the bi-modal shape with a Hoppel minimum at a diameter of about 75 nm. The Hoppel minimum vanishes for altitudes above the rain initiation level. Na and Ar_e prevailing decreased with altitude up to the cloud top. Above the cloud top, the Na increases by a factor of ~2, resulting from the detrainment of CCN particles from other clouds with higher cloud tops. This is supported by the measurements of large Ar_e resulting from the evaporation of raindrops.

3.3. 7 February 2024

Fig. 8a shows the region of aerosol and cloud vertical profile measurements on 7 February 2024. The cloud properties of clouds were measured from the cloud base to cloud top altitudes (see images of clouds in Fig. S5). The vertical profiles of aerosols were performed around clouds, which developed on marine air masses from southeasterly winds (see air masses back trajectories in Fig. S6). During this day, the atmosphere was moist at lower levels and stable with a thermal inversion at ~ 2000 m. Most clouds measured at lower levels were cumulus humulis and mediocris and stratiform clouds. In this atmospheric condition, the vertical development of clouds is suppressed, leading to the formation of cloud tops near the inversion with stratiform

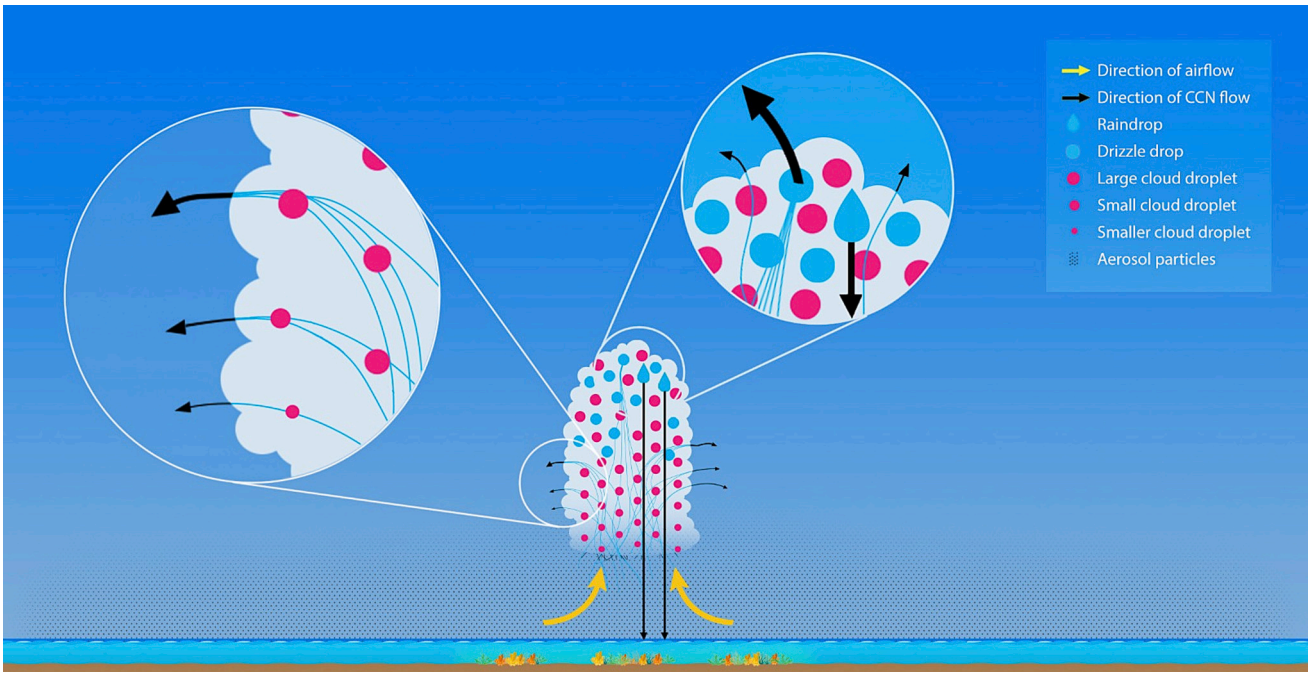

Fig. 10. General characteristics of warm clouds formed over the Great Barrier Reef (GBR) and the effect on the vertical profile of aerosols under the influence of marine air masses. CCN particles ingested below the cloud base are activated into cloud droplets. At the cloud stage, the cloud parcel contains cloud droplets and interstitial aerosols. During cloud development, cloud droplets evaporate at the lateral boundaries and above the cloud base, releasing the CCNs and the interstitial aerosol particles in the cloud-free environment. Large cloud droplets and drizzle droplets resulting from coalescence processes detrain a larger CCN particle than at the cloud base. When cloud droplets coalesce and precipitate, the CCNs that produced the coalesced cloud drops and the interstitial particles precipitate with the rain instead of detraining from the cloud.

characteristics. Furthermore, the coalescence process is suppressed, and thus, most of the aerosol particles measured around clouds result from the evaporation of relatively smaller sizes.

On this day, a larger number of cloud droplets was measured at cloud bases and above compared to the previous cases (see Fig. 8b), probably influenced by continental particles from Australian coast. The number concentration of particles measured with CPCs was larger than the Na by a factor of ~2–3, indicating that ultrafine particles were activated at cloud bases. Fig. 8b shows that light rain was measured at higher cloud depths (~ 1900 m). Note that this measurement occurred in clouds in the southern region of the spiral (while the aircraft was returning to the airport). Fig. 8c shows the vertical profile of Na, Ar_e, and the average PSDs measured with UHSAS around the clouds. The PSDs show a bi-modal shape with a Hoppel minimum diameter of about 90–100 nm from below cloud bases and above, with a relatively high concentration in the Aitken mode. The height of rain initiation was not identified in the clouds since we did not have cloud passes between 1400 m and 1900 m. The PSDs suggest that it takes place at an altitude of 1400 m. This figure indicates that the observation of the Hoppel minimum in the vertical profiles of aerosols is associated with the intensity of the coalescence processes, which capture the interstitial aerosol particles in the cloud parcel. The maximum value of RWC measured in this case was ~ 0.1 g m^{-3}. This measurement, which took place far from the spiral (see Fig. 8a), emphasizes that the height of rain initiation is the same for clouds formed in the same aerosol and thermodynamic conditions.

The scavenging effect of drizzle and raindrops in aerosol particles above cloud bases is associated with the size of the precipitating particle in clouds or the rain rate below cloud bases (Andronache, 2003; Andronache et al., 2006; Croft et al., 2009; Wang et al., 1978). For aerosol particles detrained from clouds, the resulting size distribution is affected by the scavenging of aerosols by drizzle and raindrops during cloud processing. Below cloud bases, the aerosol particle scavenging is associated with the sizes of precipitating raindrops.

3.4. 15 February 2024

Fig. 9a shows the region of aerosol and cloud vertical profile measurements on 15 February 2024 (see Fig. S7 and S8 for the cloud images and marine air masses' back trajectories). The cloud properties were measured from the cloud base to the top altitudes. The vertical profile of aerosols was performed between a precipitating cloud and growing convective cumuli. On this day, the maximum Nd measured at cloud bases was about 155 cm^{-3}, and raindrops started to be measured at ~ 950 m, with intense precipitation starting at ~ 1400 m (see Fig. 9b).

Fig. 9c shows the vertical profile of Na, Ar_e, and the average PSDs measured with UHSAS around the clouds. The PSDs show the tri-modal shape with a Hoppel minimum of about 90 nm below cloud bases. The outflow of aerosols from the precipitating clouds affected the coarse mode of aerosol particles ($d > 300$ nm). The average PSDs show that the measurements were strongly affected by the detrainment of raindrops at all altitudes, especially above the height of rain initiation. The values of Ar_e show a large range of sizes due to the measurement of evaporated raindrops, with larger sizes observed at higher altitudes.

4. Discussion

The results from measurements of the vertical profiles of aerosols around clouds and under background conditions emphasize that cloud processing dominates the aerosol properties in marine air masses over the GBR. This characteristic of aerosol properties in marine air masses as a function of cloud processing was also observed with aerosol probes of our flights during the campaign 2023 over the Heron Reef region (23.44°S, 151.88°E), not shown here due to the absence of CCP measurements (see Section S2 in the supplementary material). The marine air masses over GBR exhibited a characteristic bimodal aerosol size distribution with relatively low concentrations below cloud bases of convective and stratiform clouds. Above cloud bases, the aerosol concentrations decreased with height and showed a strong relationship with

cloud processes.

Fig. 10 summarizes the effect of warm clouds formed in marine air masses on the vertical profile of aerosols. Aerosol particles ingested from below cloud bases are partially activated into cloud droplets, decreasing the concentrations of particles above this level. At the initial cloud stage, the cloud parcel contains cloud droplets and interstitial aerosols. During cloud development, cloud droplets evaporate at the lateral boundaries and above the cloud base, releasing the CCNs and the interstitial aerosol particles in the cloud-free environment. The size of the CCN particles released from the cloud depends on the size of the droplet that has undergone evaporation. When droplet collision and coalescence processes start, drizzle droplets capture smaller droplets and interstitial aerosols. During this process, the population of detrained droplets and interstitial aerosols diminishes. The interstitial particles captured may enhance the Hoppel minimum in the initial stages of coagulation. Large raindrops are formed for intense coalescence, and the particle concentration diminishes drastically. The Hoppel minimum is not observed above this altitude. When cloud droplets coalesce and precipitate, the CCNs that produced the raindrops and the captured interstitial particles do not detrain from the cloud but are deposited to the ground. Larger aerosol particles are measured in the vertical profiles below and above cloud bases for clouds with intense precipitation developed. The particles result from the evaporation of large raindrops in the cloud's outflow.

When long-range transport (LRT) of aerosol particles is relevant above the Great Barrier Reef, the additional aerosol particles overwhelm the effect of clouds in releasing aerosol particles at their lateral boundaries. This scenario was observed in most flights during the MCB campaign 2023 in the region of Heron Reef (see Section S3 in the supplementary material). High concentrations of aerosols were measured when continental air masses blew from the east coast of Australia. The continental aerosols are transported to the free troposphere by continental-convective clouds and reach the Reef through the westerly winds at the troposphere's middle levels. Mixing LRT particles at the cloud edges may transport particles into the cloud and secondary activation of droplets. In this scenario, clouds are not the primary source of particles at higher levels of the atmosphere.

5. Conclusions

The effect of cloud droplet evaporation on aerosol concentrations around convective clouds was previously observed over the Amazon region and Atlantic Ocean by Braga et al. (2022). That study described the aerosol particle activation and deactivation dynamic at the lateral boundaries of ice-free clouds. Our observations over the GBR reinforce the hypothesis that the aerosol around the cloud is cloud-processed. Similar results were found for background conditions, indicating that the air masses reaching the GBR had been subject to cloud processing for some time prior. We show that warm clouds dominate the vertical profiles of aerosol particles at the lower troposphere over the GBR. The results from the research flights show a strong relationship between the aerosol properties and the cloud microphysical processes observed in marine clouds for similar altitudes. As the presence of a Hoppel minimum indicates, the aerosol particles found over the Reef are primarily associated with prior cloud processing. The concentration of particles decreases with height due to the activation of aerosol particles into cloud droplets and further due to collision and coalescence processes within clouds. When drizzle droplets start to form in clouds, the concentration of aerosol particles decreases at the same altitude out of clouds. Above this level, the accumulation mode particles decrease with height, leading to the absence of the Hoppel minimum observation. During this process, large aerosol particles are observed due to the detrainment of drizzle and raindrops in the open atmosphere. At altitudes above the level of intense collision and coalescence process, Aitken mode aerosol particles are predominantly detected.

Disclaimer

The opinions expressed are the authors' responsibility and not the participating institutions.

Financial support

The Reef Restoration and Adaptation Program (RRAP) and Southern Cross University have supported this research.

CRediT authorship contribution statement

Ramon C. Braga: Writing – review & editing, Writing – original draft, Methodology, Investigation, Formal analysis, Data curation, Conceptualization. **Daniel Rosenfeld:** Supervision, Investigation, Formal analysis. **Diana Hernandez:** Software, Resources, Data curation. **Chris Medcraft:** Software, Data curation. **Avichay Efraim:** Writing – review & editing, Formal analysis, Data curation. **Manuel Moser:** Writing – review & editing, Software, Data curation. **Johannes Lucke:** Software, Data curation. **Adrian Doss:** Software, Data curation. **Daniel Harrison:** Writing – review & editing, Visualization, Supervision, Resources, Project administration, Funding acquisition, Formal analysis.

Declaration of competing interest

The authors declare that they have no conflict of interest.

Acknowledgments

We thank the Reef Restoration and Adaptation Program (RRAP) and Southern Cross University, which collaborates with Australia's leading experts to create a suite of innovative and targeted measures to help preserve and restore the Great Barrier Reef.

Appendix A. Supplementary data

Supplementary data to this article can be found online at https://doi.org/10.1016/j.atmosres.2025.107928.

Data availability

The data used in this study is available at https://doi.org/10.5281/zenodo.11398223.

References

Altaratz, O., Bar-Or, R.Z., Wollner, U., Koren, I., 2013. Relative humidity and its effect on aerosol optical depth in the vicinity of convective clouds. Environ. Res. Lett. 8. https://doi.org/10.1088/1748-9326/8/3/034025.

Andreae, M.O., Crutzen, P.J., 1997. Atmospheric aerosols: biogeochemical sources and role in atmospheric chemistry. Science 1979 (276), 1052–1058. https://doi.org/10.1126/science.276.5315.1052.

Andreae, M.O., Raemdonck, H., 1983. Dimethyl sulfide in the surface ocean and the marine atmosphere: a global view. Science 1979 (221), 744–747. https://doi.org/10.1126/science.221.4612.744.

Andreae, M.O., Rosenfeld, D., 2008. Aerosol-cloud-precipitation interactions. Part 1. The nature and sources of cloud-active aerosols. Earth Sci. Rev. 89, 13–41. https://doi.org/10.1016/j.earscirev.2008.03.001.

Andreae, M.O., Rosenfeld, D., Artaxo, P., Costa, A.A., Frank, G.P., Longo, K.M., Silva-Dias, M.A.F., 2004. Smoking rain clouds over the Amazon. Science 303, 1337–1342. https://doi.org/10.1126/science.1092779.

Andronache, C., 2003. Estimated variability of below-cloud aerosol removal by rainfall for observed aerosol size distributions. Atmos. Chem. Phys. 3. https://doi.org/10.5194/acp-3-131-2003.

Andronache, C., Grönholm, T., Laakso, L., Phillips, Y., Venäläinen, A., 2006. Scavenging of ultrafine particles by rainfall at a boreal site: Observations and model estimations. Atmos. Chem. Phys. 6. https://doi.org/10.5194/acp-6-4739-2006.

Bansemer, A., 2023. System for OAP Data Analysis, Zenodo [Code]. https://doi.org/10.5281/zenodo.7803116.

Bar-Or, R.Z., Koren, I., Altaratz, O., Fredj, E., 2012. Radiative properties of humidified aerosols in cloudy environment. Atmos. Res. 118, 280–294. https://doi.org/10.1016/j.atmosres.2012.07.014.

Baumgardner, D., Jonsson, H., Dawson, W., O'Connor, D., Newton, R., 2001. The cloud, aerosol and precipitation spectrometer: a new instrument for cloud investigations. Atmos. Res. 59–60, 251–264. https://doi.org/10.1016/S0169-8095(01)00119-3.

Braga, R.C., Rosenfeld, D., Weigel, R., Jurkat, T., Andreae, M.O., Wendisch, M., Pöschl, U., Voigt, C., Mahnke, C., Borrmann, S., Albrecht, R.I., Molleker, S., Vila, D. A., Machado, L.A.T., Grulich, L., 2017. Further evidence for CCN aerosol concentrations determining the height of warm rain and ice initiation in convective clouds over the Amazon basin. Atmos. Chem. Phys. 17, 14433–14456. https://doi.org/10.5194/acp-17-14433-2017.

Braga, R.C., Ervens, B., Rosenfeld, D., Andreae, M.O., Förster, J.-D., Fütterer, D., Hernández Pardo, L., Holanda, B.A., Jurkat-Witschas, T., Krüger, O.O., Lauer, O., Machado, L.A.T., Pöhlker, C., Sauer, D., Voigt, C., Walser, A., Wendisch, M., Pöschl, U., Pöhlker, M.L., 2021a. Cloud droplet formation at the base of tropical convective clouds: closure between modeling and measurement results of ACRIDICON–CHUVA. Atmos. Chem. Phys. 21, 17513–17528. https://doi.org/10.5194/acp-21-17513-2021.

Braga, R.C., Rosenfeld, D., Krüger, O.O., Ervens, B., Holanda, B.A., Wendisch, M., Krisna, T., Pöschl, U., Andreae, M.O., Voigt, C., Pöhlker, M.L., 2021b. Linear relationship between effective radius and precipitation water content near the top of convective clouds: measurement results from ACRIDICON–CHUVA campaign. Atmos. Chem. Phys. 21, 14079–14088. https://doi.org/10.5194/acp-21-14079-2021.

Braga, R.C., Rosenfeld, D., Andreae, M.O., Pöhlker, C., Pöschl, U., Voigt, C., Weinzierl, B., Wendisch, M., Pöhlker, M.L., Harrison, D., 2022. Detrainment dominates CCN concentrations around non-precipitating convective clouds over the Amazon. Geophys. Res. Lett. 49. https://doi.org/10.1029/2022GL100411.

Cai, Y., Montague, D.C., Mooiweer-Bryan, W., Deshler, T., 2008. Performance characteristics of the ultra high sensitivity aerosol spectrometer for particles between 55 and 800 nm: Laboratory and field studies. J. Aerosol Sci. 39, 759–769. https://doi.org/10.1016/j.jaerosci.2008.04.007.

Chen, Q., Sherwen, T., Evans, M., Alexander, B., 2018. DMS oxidation and sulfur aerosol formation in the marine troposphere: a focus on reactive halogen and multiphase chemistry. Atmos. Chem. Phys. 18, 13617–13637. https://doi.org/10.5194/acp-18-13617-2018.

Croft, B., Lohmann, U., Martin, R.V., Stier, P., Wurzler, S., Feichter, J., Posselt, R., Ferrachat, S., 2009. Aerosol size-dependent below-cloud scavenging by rain and snow in the ECHAM5-HAM. Atmos. Chem. Phys. 9, 4653–4675. https://doi.org/10.5194/acp-9-4653-2009.

Eckert, C., Hernandez-Jaramillo, D.C., Medcraft, C., Harrison, D.P., Kelaher, B.P., 2024. Drone-based measurement of the size distribution and concentration of marine aerosols above the Great Barrier Reef. Drones 8. https://doi.org/10.3390/drones8070292.

Eytan, E., Koren, I., Altaratz, O., Kostinski, A.B., Ronen, A., 2020. Longwave radiative effect of the cloud twilight zone. Nat. Geosci. 13. https://doi.org/10.1038/s41561-020-0636-8.

Feingold, G., Cotton, W.R., Kreidenweis, S.M., Davis, J.T., 1999. The impact of giant cloud condensation nuclei on drizzle formation in stratocumulus: implications for cloud radiative properties. J. Atmos. Sci. 56, 4100–4117. https://doi.org/10.1175/1520-0469(1999)056<4100:TIOGCC>2.0.CO;2.

Freud, E., Rosenfeld, D., 2012. Linear relation between convective cloud drop number concentration and depth for rain initiation. J. Geophys. Res. Atmos. 117, 1–13. https://doi.org/10.1029/2011JD016457.

Gerber, H., Frick, G., 2012. Drizzle rates and large sea-salt nuclei in small cumulus. J. Geophys. Res. Atmos. 117. https://doi.org/10.1029/2011JD016249.

Gong, X., Wex, H., Müller, T., Wiedensohler, A., Höhler, K., Kandler, K., Ma, N., Dietel, B., Schiebel, T., Möhler, O., Stratmann, F., 2019. Characterization of aerosol properties at Cyprus, focusing on cloud condensation nuclei and ice-nucleating particles. Atmos. Chem. Phys. 19, 10883–10900. https://doi.org/10.5194/acp-19-10883-2019.

Gunn, R., Phillips, B.B., 1957. An experimental investigation of the effect of air pollution on the initiation of rain. J. Meteorol. 14. https://doi.org/10.1175/1520-0469(1957)014<0272:aeiote>2.0.co;2.

Haarig, M., Walser, A., Ansmann, A., Dollner, M., Althausen, D., Sauer, D., Farrell, D., Weinzierl, B., 2019. Profiles of cloud condensation nuclei, dust mass concentration, and ice-nucleating-particle-relevant aerosol properties in the Saharan Air Layer over Barbados from polarization lidar and airborne in situ measurements. Atmos. Chem. Phys. 19. https://doi.org/10.5194/acp-19-13773-2019.

Hernandez-Jaramillo, D.C., Medcraft, C., Braga, R.C., Butcherine, P., Doss, A., Kelaher, B., Rosenfeld, D., Harrison, D.P., 2024. New airborne research facility observes sensitivity of cumulus cloud microphysical properties to aerosol regime over the great barrier reef. Environ. Sci. Atmos. https://doi.org/10.1039/D4EA00009A.

Hoppel, W.A., Frick, G.M., Larson, R.E., 1986. Effect of nonprecipitating clouds on the aerosol size distribution in the marine boundary layer. Geophys. Res. Lett. 13, 125–128. https://doi.org/10.1029/GL013i002p00125.

Hoppel, W.A., Fitzgerald, J.W., Frick, G.M., Larson, R.E., Mack, E.J., 1990. Aerosol size distributions and optical properties found in the marine boundary layer over the Atlantic Ocean. J. Geophys. Res. Atmos. 95, 3659–3686. https://doi.org/10.1029/JD095iD04p03659.

IPCC, 2021. Climate Change 2021. In: The Physical Science Basis. Cambridge University Press, Cambridge.

Jackson, R.L., Gabric, A.J., Woodhouse, M.T., Swan, H.B., Jones, G.B., Cropp, R., Deschaseaux, E.S.M., 2020. Coral reef emissions of atmospheric dimethylsulfide and the influence on marine aerosols in the southern Great Barrier Reef, Australia. J. Geophys. Res. Atmos. 125. https://doi.org/10.1029/2019JD031837.

King, W.D., Parkin, D.A., Handsworth, R.J., 1978. A hot-wire liquid water device having fully calculable response characteristics. J. Appl. Meteorol. https://doi.org/10.1175/1520-0450(1978)017<1809:AHWLWD>2.0.CO;2.

Kirschler, S., Voigt, C., Anderson, B.E., Chen, G., Crosbie, E.C., Ferrare, R.A., Hahn, V., Hair, J.W., Kaufmann, S., Moore, R.H., Painemal, D., Robinson, C.E., Sanchez, K.J., Scarino, A.J., Shingler, T.J., Shook, M.A., Thornhill, K.L., Winstead, E.L., Ziemba, L. D., Sorooshian, A., 2023. Overview and statistical analysis of boundary layer clouds and precipitation over the western North Atlantic Ocean. Atmos. Chem. Phys. 23, 10731–10750. https://doi.org/10.5194/acp-23-10731-2023.

Konwar, M., Maheskumar, R.S., Kulkarni, J.R., Freud, E., Goswami, B.N., Rosenfeld, D., 2012. Aerosol control on depth of warm rain in convective clouds. J. Geophys. Res. Atmos. 117 (1–10). https://doi.org/10.1029/2012JD017585.

Konwar, M., Panicker, A.S., Axisa, D., Prabha, T.V., 2015. Near-cloud aerosols in monsoon environment and its impact on radiative forcing. J. Geophys. Res. 120, 1445–1457. https://doi.org/10.1002/2014JD022420.

Koren, I., Remer, L.A., Kaufman, Y.J., Rudich, Y., Martins, J.V., 2007. On the twilight zone between clouds and aerosols. Geophys. Res. Lett. 34. https://doi.org/10.1029/2007GL029253.

Kulkarni, J.R., Maheskumar, R.S., Morwal, S.B., Padma Kumari, B., Konwar, M., Deshpande, C.G., Joshi, R.R., Bhalwankar, R.V., Pandithurai, G., Safai, P.D., Narkhedkar, S.G., Dani, K.K., Nath, A., Nair, S., Sapre, V.V., Puranik, P.V., Kandalgaonkar, S.S., Mujumdar, V.R., Khaladkar, R.M., Vijayakumar, R., Prabha, T. V., Goswami, B.N., 2012. The cloud aerosol interaction and precipitation enhancement experiment (CAIPEEX): overview and preliminary results. Curr. Sci. 102.

Kupc, A., Williamson, C., Wagner, N.L., Richardson, M., Brock, C.A., 2018. Modification, calibration, and performance of the Ultra-High Sensitivity Aerosol Spectrometer for particle size distribution and volatility measurements during the Atmospheric Tomography Mission (ATom) airborne campaign. Atmos. Meas. Tech. 11, 369–383. https://doi.org/10.5194/amt-11-369-2018.

Lance, S., Brock, C.A., Rogers, D., Gordon, J.A., 2010. Water droplet calibration of the Cloud Droplet Probe (CDP) and in-flight performance in liquid, ice and mixed-phase clouds during ARCPAC. Atmos. Meas. Tech. 3, 1683–1706. https://doi.org/10.5194/amt-3-1683-2010.

Lopez-Yglesias, X.F., Yeung, M.C., Dey, S.E., Brechtel, F.J., Chan, C.K., 2014. Performance evaluation of the Brechtel Mfg. Humidified Tandem Differential Mobility Analyzer (BMI HTDMA) for studying hygroscopic properties of aerosol particles. Aerosol Sci. Technol. 48. https://doi.org/10.1080/02786826.2014.952366.

Lucke, J., Jurkat-Witschas, T., Heller, R., Hahn, V., Hamman, M., Breitfuss, W., Bora, V. R., Moser, M., Voigt, C., 2022. Icing wind tunnel measurements of supercooled large droplets using the 12mm total water content cone of the Nevzorov probe. Atmos. Meas. Tech. 15, 7375–7394. https://doi.org/10.5194/amt-15-7375-2022.

Mamouri, R.E., Ansmann, A., 2016. Potential of polarization lidar to provide profiles of CCN-and INP-relevant aerosol parameters. Atmos. Chem. Phys. 16. https://doi.org/10.5194/acp-16-5905-2016.

McGowan, H., Lensky, N.G., Abir, S., Saunders, M., 2022. Coral Reef coupling to the atmospheric boundary layer through exchanges of heat, moisture, and momentum: case studies from tropical and desert fringing coral reefs. Front. Mar. Sci. 9. https://doi.org/10.3389/fmars.2022.900679.

Moore, R.H., Wiggins, E.B., Ahern, A.T., Zimmerman, S., Montgomery, L., Campuzano Jost, P., Robinson, C.E., Ziemba, L.D., Winstead, E.L., Anderson, B.E., Brock, C.A., Brown, M.D., Chen, G., Crosbie, E.C., Guo, H., Jimenez, J.L., Jordan, C.E., Lyu, M., Nault, B.A., Rothfuss, N.E., Sanchez, K.J., Schueneman, M., Shingler, T.J., Shook, M. A., Thornhill, K.L., Wagner, N.L., Wang, J., 2021. Sizing response of the Ultra-High Sensitivity Aerosol Spectrometer (UHSAS) and Laser Aerosol Spectrometer (LAS) to changes in submicron aerosol composition and refractive index. Atmos. Meas. Tech. 14, 4517–4542. https://doi.org/10.5194/amt-14-4517-2021.

Moser, M., Voigt, C., Jurkat-Witschas, T., Hahn, V., Mioche, G., Jourdan, O., Dupuy, R., Gourbeyre, C., Schwarzenboeck, A., Lucke, J., Boose, Y., Mech, M., Borrmann, S., Ehrlich, A., Herber, A., Lüpkes, C., Wendisch, M., 2023. Microphysical and thermodynamic phase analyses of Arctic low-level clouds measured above the sea ice and the open ocean in spring and summer. Atmos. Chem. Phys. 23, 7257–7280. https://doi.org/10.5194/acp-23-7257-2023.

O'Dowd, C.D., de Leeuw, G., 2007. Marine aerosol production: a review of the current knowledge. Philos. Trans. R. Soc. A Math. Phys. Eng. Sci. 365, 1753–1774. https://doi.org/10.1098/rsta.2007.2043.

Quinn, P.K., Coffman, D.J., Johnson, J.E., Upchurch, L.M., Bates, T.S., 2017. Small fraction of marine cloud condensation nuclei made up of sea spray aerosol. Nat. Geosci. 10, 674–679. https://doi.org/10.1038/ngeo3003.

Reutter, P., Su, H., Trentmann, J., Simmel, M., Rose, D., Gunthe, S.S., Wernli, H., Andreae, M.O., Pöschl, U., 2009. Aerosol- and updraft-limited regimes of cloud droplet formation: influence of particle number, size and hygroscopicity on the activation of cloud condensation nuclei (CCN). Atmos. Chem. Phys. 9, 7067–7080. https://doi.org/10.5194/acp-9-7067-2009.

Rogers, R.R., Yau, M.K., 1989. A Short Course of Cloud Physics, Third ed. Library of Congress, Oxford, UK.

Rosenfeld, Daniel, 2018. Cloud-Aerosol-Precipitation Interactions Based of Satellite Retrieved Vertical Profiles of Cloud Microstructure. https://doi.org/10.1016/B978-0-12-810437-8.00006-2.

Rosenfeld, D., Lahav, R., Khain, A., Pinsky, M., 2002. The role of sea spray in cleansing air pollution over ocean via cloud processes. Science 297, 1667–1670. https://doi.org/10.1126/science.1073869.

Rosenfeld, D., Lohmann, U., Raga, G., 2008. Flood or drought: how do aerosols affect precipitation? Science 1979 (321), 1309–1313.

Stein, A.F., Draxler, R.R., Rolph, G.D., Stunder, B.J.B., Cohen, M.D., Ngan, F., 2015. Noaa's hysplit atmospheric transport and dispersion modeling system. Bull. Am. Meteorol. Soc. https://doi.org/10.1175/BAMS-D-14-00110.1.

Swan, H.B., Crough, R.W., Vaattovaara, P., Jones, G.B., Deschaseaux, E.S.M., Eyre, B.D., Miljevic, B., Ristovski, Z.D., 2016. Dimethyl sulfide and other biogenic volatile organic compound emissions from branching coral and reef seawater: potential sources of secondary aerosol over the Great Barrier Reef. J. Atmos. Chem. 73, 303–328. https://doi.org/10.1007/s10874-016-9327-7.

Twomey, S., 1959. The nuclei of natural cloud formation part II: the supersaturation in natural clouds and the variation of cloud droplet concentration. Geofis. Pura Appl. 43, 243–249. https://doi.org/10.1007/BF01993560.

Wang, P.K., Grover, S.N., Pruppacher, H.R., 1978. On the effect of electric charges on the scavenging of aerosol particles by clouds and small raindrops. J. Atmos. Sci. 35. https://doi.org/10.1175/1520-0469(1978)035<1735:oteoec>2.0.co;2.

Wang, J., McNeill, V.F., Collins, D.R., Flagan, R.C., 2002. Fast mixing condensation nucleus counter: Application to rapid scanning differential mobility analyzer measurements. Aerosol Sci. Technol. 36. https://doi.org/10.1080/02786820290038366.

Wex, H., Dieckmann, K., Roberts, G.C., Conrath, T., Izaguirre, M.A., Hartmann, S., Herenz, P., Schäfer, M., Ditas, F., Schmeissner, T., Henning, S., Wehner, B., Siebert, H., Stratmann, F., 2016. Aerosol arriving on the Caribbean island of Barbados: physical properties and origin. Atmos. Chem. Phys. 16, 14107–14130. https://doi.org/10.5194/acp-16-14107-2016.

Wollesen De Jonge, R., Elm, J., Rosati, B., Christiansen, S., Hyttinen, N., Lüdemann, D., Bilde, M., Roldin, P., 2021. Secondary aerosol formation from dimethyl sulfide-improved mechanistic understanding based on smog chamber experiments and modelling. Atmos. Chem. Phys. 21, 9955–9976. https://doi.org/10.5194/acp-21-9955-2021.